EUROPEAN ORGANIZATION FOR NUCLEAR RESEARCH

CERN-EP/89-111
31 August 1989

INCLUSIVE NEGATIVE PARTICLE $p_\perp$ SPECTRA IN p-NUCLEUS AND NUCLEUS-NUCLEUS COLLISIONS AT 200 GeV PER NUCLEON

HELIOS COLLABORATION

T. Åkesson[3], S. Almehed[3], A.L.S. Angelis[19], N. Armenise[1], H. Atherton[3], P. Aubry[8], H.W. Bartels[4], G. Beaudoin[8], J.M. Beaulieu[8], H. Beker[3], O. Benary[18], D. Bettoni[3,a], V. Bisi[19], I. Blevis[21], H. Bøggild[3,b], W. Cleland[12], M. Clemen[12], B. Collick[12], F. Corriveau[7], S. Dagan[18], K. Dederichs[3,c], S. Dell'Uomo[13], P. Depommier[8], R.C.E. Devenish[3,d], S. Di Liberto[13], N. DiGiacomo[5], J.R. Dodd[20], B. Dogolshein[10], A. Drees[4], H. En'yo[3], B. Erlandsson[17], M.J. Esten[20], C.W. Fabjan[3], P. Fischer[4], Z. Fraenkel[21], A. Gaidot[15], F. Gibrat-Debu[15], P. Giubellino[19], P. Glässel[4], U. Goerlach[4], R. Haglund[6], L.A. Hamel[7], H. van Hecke[5], V. Hedberg[3], R. Heifetz[18], A. Hölscher[4], B. Jacak[5], G. Jarlskog[6], S. Johansson[6], H. Kraner[2], V. Kroh[4], F. Lamarche[7], C. Leroy[7], D. Lissauer[2,18], G. London[15], B. Lörstad[6], A. Lounis[8], F. Martelli[19,22], A. Marzari-Chiesa[19], M. Masera[19], M.A. Mazzoni[3], E. Mazzucato[7], M.L. McCubbin[19], N.A. McCubbin[14], P. McGaughey[5], F. Meddi[13], U. Mjörnmark[6], M.T. Muciaccia[1], S. Muraviev[9], M. Murray[12], M. Neubert[4], S. Nilsson[17], L. Olsen[2], Y. Oren[18], J.P. Pansart[15], Y.M. Park[12], A. Pfeiffer[4], F. Piuz[3], V. Polychronakos[2], G. Poulard[3], M. Price[3], D. Rahm[2], L. Ramello[19], L. Riccati[19], G. Romano[16], G. Rosa[13], L. Sandor[3], J. Schukraft[3], M. Sekimoto[3,e], B. Sellden[17], M. Seman[3,f], A. Shmeleva[9], V. Sidorov[11], S. Simone[1], Y. Sirois[7], H. Sletten[3], S. Smirnov[10], J. Soltani[4], W. Sondheim[5], H.J. Specht[4], I. Stumer[2], J. Sunier[5], V. Tcherniatin[10], H.H. Thodberg[3], J. Thompson[12], V. Tikhomirov[9], I. Tserruya[21], G. Vasseur[15], R. Veenhof[3,g], R. Wigmans[3,g], P. Yepes[7]

(Submitted to Z. Physik C)

1) University of Bari and INFN, Bari, Italy
2) Brookhaven National Lab., Upton, NY, USA
3) CERN, Geneva, Switzerland
4) University of Heidelberg, Fed. Rep. Germany
5) Los Alamos Nat. Lab., Los Alamos, NM, USA
6) University of Lund, Sweden
7) McGill University, Montreal, Canada
8) University of Montreal, Canada
9) Lebedev Phys. Inst., Moscow, USSR
10) Phys. Eng. Inst., Moscow, USSR
11) Inst. Nucl. Phys., Novosibirsk, USSR
12) University of Pittsbourgh, Pittsbourgh, USA
13) University of Rome and INFN, Rome, Italy
14) Rutherford Appleton Laboratory, Didcot, UK
15) DPhPE, CEN-Saclay, Gif-sur-Yvette, France
16) University of Salerno and INFN, Salerno, Italy
17) University of Stockholm, Sweden
18) University of Tel Aviv, Israel
19) University of Turin and INFN, Turin, Italy
20) University College, London, UK
21) Weizmann Institute, Rehovot, Israel
22) Angelo Della Riccia fellow

Visitors at CERN from:
a) University of Syracuse, Syracuse, NY, USA
b) Niels Bohr Institute, Copenhagen, Denmark
c) University of Munich, Fed. Rep. Germany
d) University of Oxford, UK
e) Insitute of Nuclear Study, Tokyo, Japan
f) Slovak Academy of Sciences, Kosice, Czechoslovakia
g) NIKHEF-H, Amsterdam, The Netherlands

Abstract

The HELIOS experiment has measured inclusive $p_\perp$ spectra of negative particles in the rapidity region $1.0 < y < 1.9$. The general shape of the $p_\perp$ spectra in p+W, O+W and S+W is similar, but cannot be described by a single exponential. Compared to p+p collisions, an excess is observed for low and high $p_\perp$. This effect increases with the projectile mass. Except for very low $E_\perp$, the average transverse momentum $\langle p_\perp \rangle$ is found to be approximately constant up to the highest accessible values of $E_\perp$.

1. Introduction

The study of hadron production in heavy ion collisions is essential to the search for effects beyond independent nucleon-nucleon collisions, for example the predicted quark gluon plasma [1]. Hadron distributions are known over a large range of transverse momenta for p+p collisions, thus a search for differences can be made. The $p_\perp$ spectra of hadrons from nucleus-nucleus collisions may indicate the degree of thermalization reached, and provide evidence for collective expansion of the highly excited central region and thus, at least indirectly, for the deconfinement transition [2,3,4,5,6].

The HELIOS (High Energy Lepton and Ion Spectrometer) experiment combines 4π calorimeter coverage with measurement of charged particle multiplicities, inclusive particle distributions, photons and lepton pairs. Single particles are detected with a magnetic spectrometer examining the event through a narrow azimuthal gap in the calorimeter. This device allows the study of particle composition, charged particle and photon momentum spectra, and a search for rare particles, such as antiprotons. In this paper we present results on negative particles, dominantly pions, from 200 GeV per nucleon p+W, O+W and S+W, S+Pt.

2. The Experimental Setup

The external spectrometer (Fig. 1) views the target through a horizontal slit in the calorimeter wall, covering the pseudorapidity interval $1.0 < \eta < 1.9$. To support the calorimeter, the slit is filled with aluminum hexcel, with a thickness of 3% radiation length. The slit measures 10 cm vertically, varying the azimuthal coverage of the spectrometer from 2.1% at $\eta = 1.9$ to 0.75% at $\eta = 1.0$.

A magnet with a momentum kick of 80 MeV/c and two high-resolution drift chambers (DC4, DC5) provide the momentum measurement of charged particles. Each chamber has 8 parallel sense wire planes, yielding up to 8 space points per track on either side of the magnet. The horizontal coordinate is measured via the drift time ($\sigma_x \sim 200\ \mu m$), and the vertical coordinate via charge division ($\sigma_y \sim 1.0\ cm$). To resolve left/right ambiguities, the sense wires are staggered by 200 μm. For the sulfur run, the readout is done with FADC's. A time-of-flight scintillator hodoscope (TOF) and an aerogel cherenkov counter ($\check{\mathrm{C}}$) are used for particle identification. In front of DC4, a 1 mm iron converter, bracketed by two multi-wire proportional chambers (COMET), allows identification and measurement of photons via the conversion method. The total material before the drift chambers adds up to $\sim$ 10% radiation length.

Collisions are sorted according to impact parameter using the transverse energy measured in the calorimeters [7]. Selection of high-$E_\perp$ events selects small impact

parameter collisions, with high energy deposition in the target. Varying scale-down factors at the trigger level ensure uniform statistical coverage over the entire $E_\perp$ range. A minimum multiplicity in a silicon counter system [7] immediately downstream of the target provides a pretrigger for the $E_\perp$ selection and serves as a minimum-bias trigger. To enrich the number of minimum-bias events with a track in the external spectrometer, there is an other trigger requiring hits in the time-of-flight hodoscope. A comparison of the multiplicity distribution taken with this trigger and the minimum-bias trigger showed no significant bias.

3. Data Analysis

For the p+W and S+Pt data sets, an active target is used [8] in which the 16 potential wires of a drift chamber serve as the targets. Ref. [8] includes also more details on the data analysis. The readout with FADC's gives a projection of the event. The ionisation maximum in a narrow window around the beam signal is used to find the target wire at which the interaction took place. Fig. 2 shows the good correlation between the vertex position found in the active target and the mean reconstructed target position of tracks in the external spectrometer. The number of reconstructed interactions per target wire as function of $E_\perp$ indicates about 50% double interactions at very high $E_\perp$ in S+Pt events, though a comparison of interactions at the first and last target wires as a function of $E_\perp$ shows that double interactions do not influence the $p_\perp$ spectra. To reduce the double interactions to a safe level below 10%, only interactions at the last 4 target wires were used. Half of the sulfur events with $E_\perp > 230$ GeV are accumulated with the active target. The other data sets are from disk targets. The available statistics of negative tracks and the targets used for the different data sets are summarized in Table I.

Table I

system	negative tracks	target
p+W	12000	active 1.0 mm wires
O+W	21000	disk 0.1 mm
S+W	91000	disk 0.2 mm
S+Pt	11500	active 0.2 mm wires

Track reconstruction and momentum measurement are performed in several steps. The coordinate system has the z-axis along the 15° line (see Fig. 1), the x-axis parallel to the drift chambers and the y-axis perpendicular to the x-z plane. In the first step, track segments are reconstructed in the x-z plane for each drift chamber, requiring at least 4

of the 8 possible hits within a road of $2\sigma_x$. Individual segments are extrapolated to the center plane between the drift chambers; those that match within 10 cm are marked as track candidates. A track fit using the drift chamber information alone allows rejection of random segment combinations by a χ^2 cut.

The tracks are extrapolated back to the target. Cuts on the horizontal ($x < \pm$ 10 cm) and vertical intercepts ($y < \pm$ 15 cm) at the target are used to separate tracks originating at the target from calorimeter background. The distributions of these intercepts are shown in Fig. 3 together with a Monte Carlo simulation. Due to the observed non-Gaussian y-resolution, which was not perfectly simulated, the Monte Carlo fails to describe the tails at y $> \pm$10 cm. A Monte Carlo study of the slit indicates that less then 2% of the tracks satisfying the target pointing requirement arise from calorimeter background. This background has a small momentum dependence showing a maximum contribution of approximately 4% at 1.5 GeV/c.

The momentum reconstruction is performed using the drift chamber information and the target position, taking into account multiple scattering between the target and the drift chambers. This multiple scattering is calculated using an estimate of the momentum from the slopes of the two track segments. Below 1 GeV/c, multiple scattering is large, essentially excluding the target point from the fit. The momentum resolution is then limited by the drift chamber resolution resulting in $\delta p/p^2 = 0.08$. Above 1 GeV/c, the momentum resolution is $\delta p/p = 0.12$, limited by the multiple scattering. At very high momenta, beyond the range of momenta studied here, the bending angle is small and the drift chamber resolution again dominates the momentum resolution.

The measured transverse momentum spectra are corrected by a Monte Carlo simulation of various detector effects including geometric acceptance, reconstruction efficiency, the finite momentum resolution and decays in flight. Pions were generated using a parameterization based on CERN ISR p+p measurements [9,10] of charged particle $p_\perp$ spectra, taking into account the dependence on the center-of-mass energy. The parameterization was modified to include the high-$p_\perp$ excess effect observed in p-nucleus collisions [11]:

$$\frac{d\sigma_{pA}}{dp_\perp} = A^{n(p_\perp)} \frac{d\sigma_{pp}}{dp_\perp}$$

where n($p_\perp$) varies approximately linearly with $p_\perp$ for $0.8 < p_\perp < 3$ GeV/c. The rapidity distribution was taken from $dE_\perp/d\eta$ measured by HELIOS [7], which is consistent with the rapidity distribution of negative particles in our acceptance. The parameters were tuned to fit the measured data. These simulated events were reconstructed using the full analysis chain. The ratio of generator input to reconstructed Monte-Carlo spectra was used to correct the data.

The external spectrometer has a fixed acceptance in pseudorapidity, therefore the pion rapidity acceptance depends on $p_\perp$ (Fig. 4). Spectra are presented in a fixed rapidity

range, $1.0 < y < 1.9$. The low-$p_\perp$ cutoff is 75 MeV/c. A correction is done for low-$p_\perp$ particles with $y > 1.4$ using the same rapidity distribution as for $p_\perp > 300$ MeV/c. In calculating the rapidity, all negative particles are assumed to be pions, neglecting kaons, as the K^-/π^- ratio measured in the spectrometer with the time-of-flight is of the order of a few percent [12]. Fig. 5 shows the correction factors as a function of $p_\perp$. They steeply rise towards low $p_\perp$, reflecting the rapid acceptance change in this region. Above 200 MeV/c, they change only slightly. During the sulfur run, the drift chambers were operated with higher gain, increasing their efficiency (curve labelled 'high gain' in Fig. 5).

The low-$p_\perp$ part of the spectrum is corrected for photon conversions in the upstream material. These photons arise from meson decays, predominantly π^0. We assume that the π^0 $p_\perp$ spectrum is the same as that for π^-. The contribution of electrons is estimated to be ~20% at 75 MeV/c by a Monte Carlo study. This correction was verified by a measurement of e^-/π^- in a limited sample of S+W interactions [12]. Decay corrections are made under the assumption that the detected negative particles are pions. Most muons from kaon decays do not point back to the target. Other instrumental effects in the reconstruction of low-$p_\perp$ tracks, such as multiple scattering and energy loss have been simulated in the Monte Carlo program, and result in small corrections to the spectrum.

The relation of drift time vs. position is uncertain to $\sim 1\%$, resulting in a momentum-dependent systematic error of at most 5% at $p_\perp = 2$ GeV/c. The distortion of the nearly exponential spectrum arising from the finite momentum resolution is corrected with an accuracy of 5% at 2 GeV/c, limited by the knowledge of the total thickness of the material in front of the drift chambers. At high $p_\perp$ an uncertainty of 250 μm in the relative position of the target and the two drift chambers in the x-direction yields the largest systematic error of 10% at 2 GeV/c. The correction for photon conversion gives an additional systematic uncertainty of 4% in the cross section at low $p_\perp$. Other effects have much smaller contributions, leading to the overall systematic error of 8% below 0.2 MeV/c, 3% up to 1 GeV/c, rising to 5% at 1.5 GeV/c and 20% at 2.5 GeV/c. It should be noted that this results in an error in the slope of the $p_\perp$ spectra of less than 3%. The uncertainty of the absolute normalization is approximately 30%, limited by the knowledge of the chamber and track reconstruction efficiency.

4. Inclusive Negative-Particle $p_\perp$ Spectra for central collisions

Fig. 6 shows the transverse momentum spectra $d\sigma/dp_\perp^2$ for negative particles in p+W, O+W and S+W collisions. The errors shown are purely statistical (as in the following figures). The spectra do not correspond to minimum bias events, but reflect the different thresholds in transverse energy $E_\perp$ ($-0.1 < \eta < 2.9$) for different projectiles: $E_\perp > 80$,

60, 10 GeV for S+W , O+W and p+W , respectively. These thresholds correspond to about 25% of the geometrical cross section. The $p_\perp$ spectra clearly cannot be described by a single exponential. The measured inverse slope for S+W data, fitted to exponential distributions in limited $p_\perp$ ranges are 210 MeV/c for the region $0.5 < p_\perp < 1.5$ GeV/c, and 85 MeV/c for $0.075 < p_\perp < 0.25$ GeV/c.

The rise in cross section at low $p_\perp$ has been reported at more central rapidities in heavy-ion collisions at CERN [13], in p-nucleus collisions at Fermilab [14], for cosmic ray data [15], and in heavy-ion collisions at BEVALAC energies [16]. At more central rapidities, the effect seems somewhat smaller than in our spectrometer, which extends into the target rapidity region. We have investigated the rapidity dependence and find no significant change of the slope for $0.075 < p_\perp < 0.25$ GeV/c within the rapidity region $1.0 < y < 1.4$, which is, however, a rather small rapidity window.

In Fig. 6a, the $p_\perp$ spectrum from p+W is compared to the parameterization of minimum-bias p+p data discussed above (full line) [9,10]. An increased production of particles at high $p_\perp$ in p-nucleus collisions, first observed by Cronin et al. [11], is evident. From Figs. 6b and 6c, it is clear that the spectra of nucleus-nucleus collisions closely resemble those from p-nucleus collisions, and a similar enhancement at high $p_\perp$ occurs.

Fig. 7 compares the shapes of the $p_\perp$ spectra from different projectiles by plotting ratios of the spectra as a function of $p_\perp$. The ratios are normalized to unity in the range $0.25 < p_\perp < 0.5$ GeV/c, since the absolute ratio is not meaningful for data taken with different $E_\perp$-thresholds. A clear projectile dependence is observed. Both σ_{SW}/σ_{pW} and, to a lesser extent, σ_{OW}/σ_{pW} deviate from unity. For the larger projectile, the production of particles with $p_\perp > 1.3$ GeV/c is larger. The projectile dependence is also visible in the mean transverse momentum, when the values of $\langle p_\perp \rangle$ are determined in the range 0.4 to 2.0 GeV/c. $\langle p_\perp \rangle$ is calculated in the given range, then extrapolated to the mean of the entire spectrum under the assumption of a purely exponential shape. The requirement $p_\perp > 400$ MeV/c excludes the low-$p_\perp$ rise; thus the result may be compared to p+p collisions. The $\langle p_\perp \rangle$ values obtained can, however, be affected by deviations in the spectral shape from exponential. We find $\langle p_\perp \rangle = 413 \pm 5$, 408 ± 10 and 372 ± 10 MeV/c for S+W, O+W and p+W respectively, all with an additional systematic error of 10 MeV/c.

In p+p and p+A collisions, $\langle p_\perp \rangle$ for pions varies with rapidity [17]. We have determined that for S+W data $\langle p_\perp \rangle$ decreases by 30 ± 10 MeV/c, going from $1.45 < y \leq 1.9$ to $0.9 < y \leq 1.45$. Within errors, this effect does not change the projectile dependence of the $p_\perp$ distribution.

5. $E_\perp$ Dependence

In this section the $E_\perp$ dependence of negative particle $p_\perp$ spectra is investigated. Since the spectra for S+W and S+Pt show no difference within the statistical accuracy, they are combined to enlarge the accessible range of $E_\perp$.

Fig. 8 presents ratios of negative particle spectra in consecutive $E_\perp$ intervals for S+W/Pt, normalized to the spectrum measured for $180 < E_\perp < 240$ GeV. $E_\perp$ is measured in $-0.1 < \eta < 2.9$. Events with $E_\perp > 180$ GeV represent only 10% of the cross section, and include the most central collisions [7]. Fig. 8 therefore provides a comparison of collisions ranging from peripheral to the most central. In the lowest $E_\perp$ range, $30 < E_\perp < 60$ GeV, a subtraction of non-target interactions (50% of the total), measured with an empty target holder, was necessary. The spectrum in this range is somewhat softer in the region $0.6 < p_\perp < 2$ GeV/c; similar results are reported in ref. [18]. For all other $E_\perp$-bins, the $p_\perp$ spectra clearly do not change.

In order to characterize the charged particle spectra over the entire range of impact parameters and different projectiles, Fig. 9 shows $\langle p_\perp \rangle$ (defined in section 4.) as a function of $E_\perp$. For sulfur data, $\langle p_\perp \rangle$ rises by 50 MeV/c from peripheral collisions to those with substantial overlap of the target and projectile. It then remains approximately constant up to very central collisions in which the highest energy densities are achieved. A constant $\langle p_\perp \rangle$ is observed for O+W and p+W collisions (Figs. 9b and c) in the $E_\perp$ range shown, which does not include peripheral collisions.

6. Discussion and Conclusion

As shown in Fig. 6, the $p_\perp$ spectrum in p-nucleus collisions deviates from pp collisions. At low $p_\perp$, we observe a striking difference in the cross section for p-nucleus and nucleus-nucleus collisions compared to pp interactions. It is important to note that the pions with $p_\perp < 250$ MeV/c represent the dominant fraction of the pion production. The rapidity dependence may help distinguish among possible production mechanisms. Low-$p_\perp$ pions produced by rescattering in the target or from the decays of Δ and N^* resonances should be observed close to the target rapidity, in contrast to a central-rapidity source undergoing a collective transverse expansion, such as proposed in reference [15]. The recent suggestion [19] that very soft pions may be produced through an intermediate system of cold, non-thermal partons also implies central production of low-$p_\perp$ pions. Within our range $1 < y < 1.4$, the low-$p_\perp$ component does not change, though the interval may be too narrow to see any change.

The increase at high-$p_\perp$ can be associated with the 'anomalous enhancement' of high-$p_\perp$ hadron production in p-nucleus interactions, discovered by Cronin et al. [11]. They found that the inclusive cross section can be parameterized by a power law dependence on the target mass A, $d\sigma/dp_\perp^2 \sim A^{n(p_\perp)}$. We observe a similar high-$p_\perp$ excess in nucleus-

nucleus over p-nucleus collisions which can be parameterized in terms of the projectile mass as $(AB)^{n(p_\perp)}$. Figure 10 shows $n(p_\perp)$ extracted from the ratios in figure 7. It is in good agreement with a parameterization of $n(p_\perp)$ measured in p-nucleus collisions at FNAL [11,14] (solid line). This can be interpreted as a dependence of the Cronin effect on the projectile analogous to that on the target.

It has been suggested that the Cronin effect is due to rescattering of partons [20] or pions in the target nucleus. This must lead to a stronger enhancement of high $p_\perp$ particles at target rapidities compared to central rapidities. A possible rapidity dependence of the enhancement may therefore indicate whether the Cronin effect is connected with rescattering. In our restricted range $1.0 < y < 1.9$, however, no rapidity dependence is observed.

Apart from the lowest bin in $E_\perp$ for S+W, 45 GeV, the average transverse momentum $\langle p_\perp \rangle$ is found to be practically independent of $E_\perp$ up to extreme central collisions, i.e. those with the highest energy densities. The initial rise with $E_\perp$ may again reflect the Cronin effect, i.e. a rise of $\langle p_\perp \rangle$ with the number of participants in the region of peripheral collisions. The constancy of $\langle p_\perp \rangle$ at higher $E_\perp$ can be interpreted either in hydrodynamic models or in microscopic models. Hydrodynamic models have, moreover, the option of assuming a hadron-parton phase transition or a pure hadron phase. In case of a phase transition, a constant $\langle p_\perp \rangle$ is obtained from the coexistence stage of the two phases in a natural way, due to the constant temperature and the constant pressure, i.e. the absence of strong hydrodynamical expansion effects at energy densities not too high above the critical density [2,5,21]. In case of a pure hadron system, assuming (i) the hadrons to always decouple at the same number density, i.e. the same temperature independent of the initial state, and assuming (ii) that there is only longitudinal hydrodynamical expansion, a constant $\langle p_\perp \rangle$ can also be obtained. Numerical calculations for a pure hadron phase [5], however, do also show transverse expansion effects, resulting in a $\langle p_\perp \rangle$ rise of about 30% over the lever arm in energy density reached in this experiment. Microscopic models, finally, can give approximately constant $\langle p_\perp \rangle$, since the hadronisation process masks the increased $\langle p_\perp \rangle$ of the partons with increasing number of parton interactions leading to higher $E_\perp$.

Thus, the interpretation of the observed constant $\langle p_\perp \rangle$ remains somewhat ambiguous. It should, in any case, be stressed that the isolation of transverse expansion effects from the *shape* of the transverse momentum spectra alone remains questionable as long as the observed excess at low $p_\perp$ and the Cronin effect (at high $p_\perp$) are not simultaneously accounted for.

Acknowledgement: The HELIOS Collaboration acknowledges the outstanding performance of the PS-SPS accelerator complex. The dedication of the CERN Accelerator Division staff is most appreciated. We thank the staff of the GSI computer center for the resources and invaluable help in data analysis. We are grateful for support by the Natural Science and Engineering Research Council of Canada, the Institut de Recherche Fondamentale (CEA, France) the German Federal Minister for Research and Technology, the US-Israel Binational Science Foundation, the Instituto Nazionale di Fisica Nucleare of Italy, the Science Research Council of the United Kingdom and the US Department of Energy.

References

1. See, for example, Proc. of the Quark Matter Conferences in Brookhaven (1984), Helsinki (1985), Asilomar (1986), Nordkirchen (1987) and Lenox (1988)
2. L. van Hove, Z.Phys.C27, 135(1985).
3. K. Redlich and H. Satz, Phys. Rev. D33, 3747 (1986).
4. K.S. Lee and U. Heinz, Univ. Regensburg preprint TPR-88-16, (1988).
5. M. Kataja, P.V. Ruuskanen, L. Mc Lerran and H. von Gersdorff, Phys. Rev. D34, 2755 (1986).
6. X. Wang and R. Hwa, Phys. Rev. D35, 3409 (1987).
7. T. Åkesson et al., Z. Phys. C38, 383 (1988),

   T. Åkesson et al., Phys. Lett. B214 , 295 (1988).
8. A. Drees, Dissertation Universität Heidelberg, (1989).
9. B. Alper et al., Nucl. Phys. B100, 237 (1975).
10. H. Bøggild, HELIOS Note 369 (1988), unpublished.
11. J. W. Cronin et al., Phys. Rev. D11, 3105 (1975).

    D. Antreasyan et al., Phys. Rev. D19, 764 (1979).
12. T. Åkesson et al., to be published.
13. H. Stroebele et al., Z. Phys. C38, 89 (1988).
14. D. A. Garbutt et al., Phys. Lett. 67B, 355 (1977).
15. T.W. Atwater, P.S. Freier and J.I. Kapusta, Phys. Lett. 199B, 30 (1987).
16. R. Brockmann et al., Phys. Rev. Lett. 53, 2012 (1984),

    G. Odyniec et al., Proc. of the 8th High Energy Heavy Ion Study, LBL 24580, 215 (1987).
17. A. Breakstone et al., Europhys. Lett. 7(2), 131 (1988).
18. R. Albrecht et al., submitted to Z. Phys. (1989).
19. L. van Hove, CERN-TH. 5236/88
20. M. Lev and B. Petersson,Z.Phys.C21, 155 (1983).
21. E. V. Shuryak, Z.Phys.C38, 165 (1988).

Figure captions

Fig. 1 Experimental setup of the external spectrometer in the HELIOS experiment (1987).

Fig. 2 Mean target vertex derived from extrapolated tracks in the external spectrometer vs. target wire as identified by the active target algorithm

Fig. 3 Resolution of the target pointing in horizontal (x) and vertical (y) direction for S+W. The cuts ensuring tracks from the target are indicated. Closed squares: data; histogram: Monte-Carlo

Fig. 4 Acceptance ($16° < \theta < 42.5°$) for pions in a $p_\perp$ -rapidity plane. The low momentum cutoff at 200 MeV/c is indicated as a dashed line. The hatched area shows the region $1.0 < y < 1.9$ and $0.075 < p_\perp < 2.5$ GeV/c for which the data are presented.

Fig. 5 Monte Carlo derived correction factors vs. $p_\perp$. The factors are used to correct the $p_\perp$ spectra for geometrical acceptance, efficiency, decays in flight, multiple scattering and finite momentum resolution, including the extrapolation to correct for low-$p_\perp$ particles lost due to the fixed angular acceptance (Fig 4). The difference between 'low gain' and 'high gain' is explained in the text.

Fig. 6 $d\sigma/dp_\perp^2$ is shown for central collisions of p, O and S (top to bottom) with a W target. Central collisions are selected by a cut in transverse energy $E_\perp$ $>$ 10, 60, and 80 GeV, respectively. For comparison, a parameterization of pp data (see text) is shown as a full line.

Fig. 7 Ratios of the spectra shown in Fig 6. Since different $E_\perp$ thresholds are used, the ratios are normalized to unity.

Fig. 8 Ratios of S+W $p_\perp$ spectra in different regions of $E_\perp$. Central collisions ($180 < E_\perp < 240$ GeV) are used for reference. The spectra are normalized to unity.

Fig. 9 $\langle p_\perp \rangle$ is shown as a function of $E_\perp$ ($-0.1 < \eta < 2.9$). The mean as determined in the range $0.4 < p_\perp < 2.0$ GeV/c is converted to $\langle p_\perp \rangle$ for the full range assuming an exponential shape. (a) combined data set of S+W and S+Pt , (b) O+W and (c) p+W.

Fig. 10 The ratios in Fig. 7 are used to extracted n($p_\perp$), assuming a parameterization $\sigma_{AB}(p_\perp) \sim (AB)^{n(p_\perp)}\sigma_{pp}$. n($p_\perp$) is known up to a constant, which was chosen such that the data can be compared with measurements of n($p_\perp$) in pA collisions at FNAL [11,14] shown as solid line.

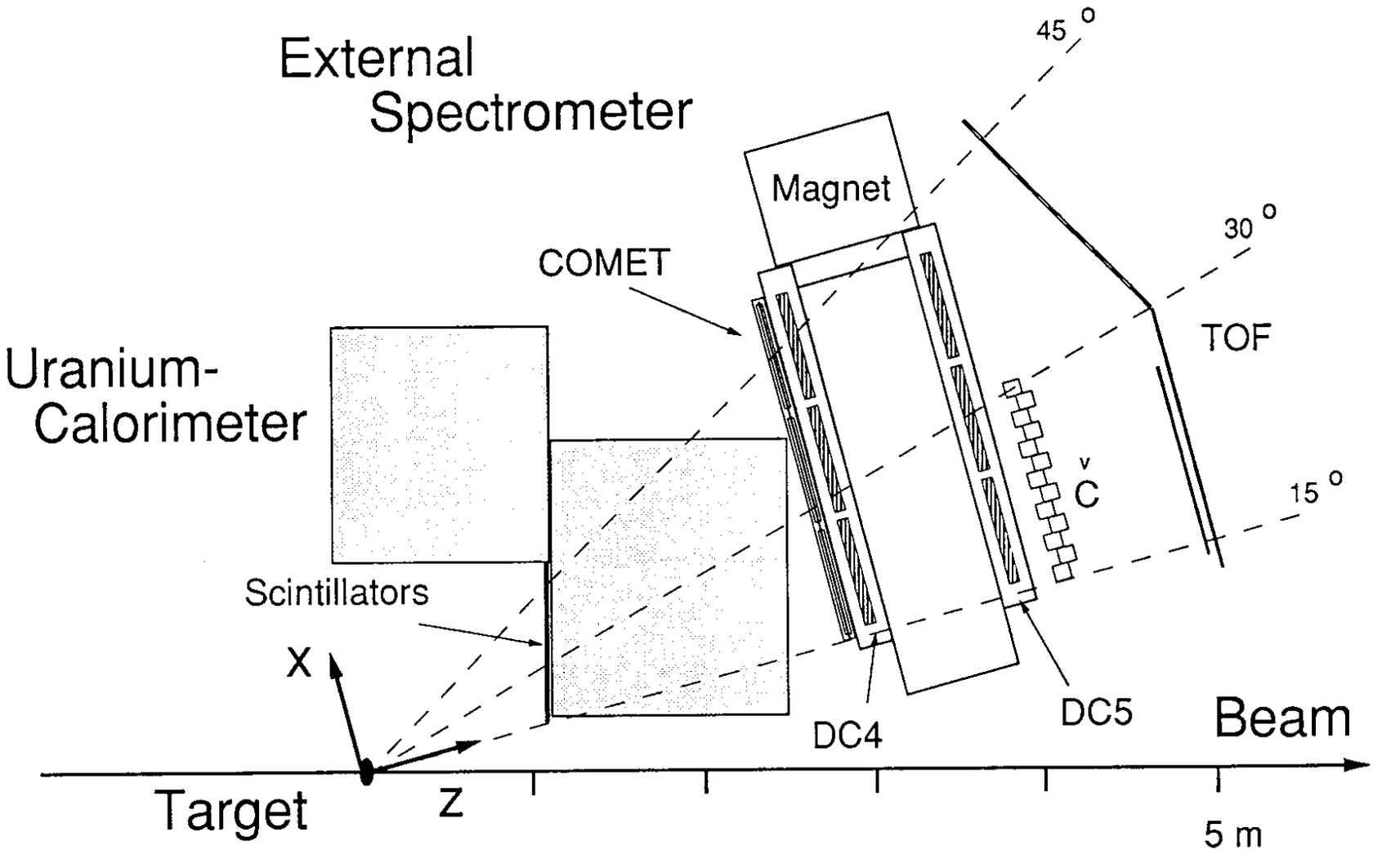
External
Spectrometer
45 °
Magnet
30 °
COMET
TOF
Uranium-
Calorimeter
C
v
15 °
Scintillators
X
DC4
DC5
Beam
Target
z
5 m

Fig. 1

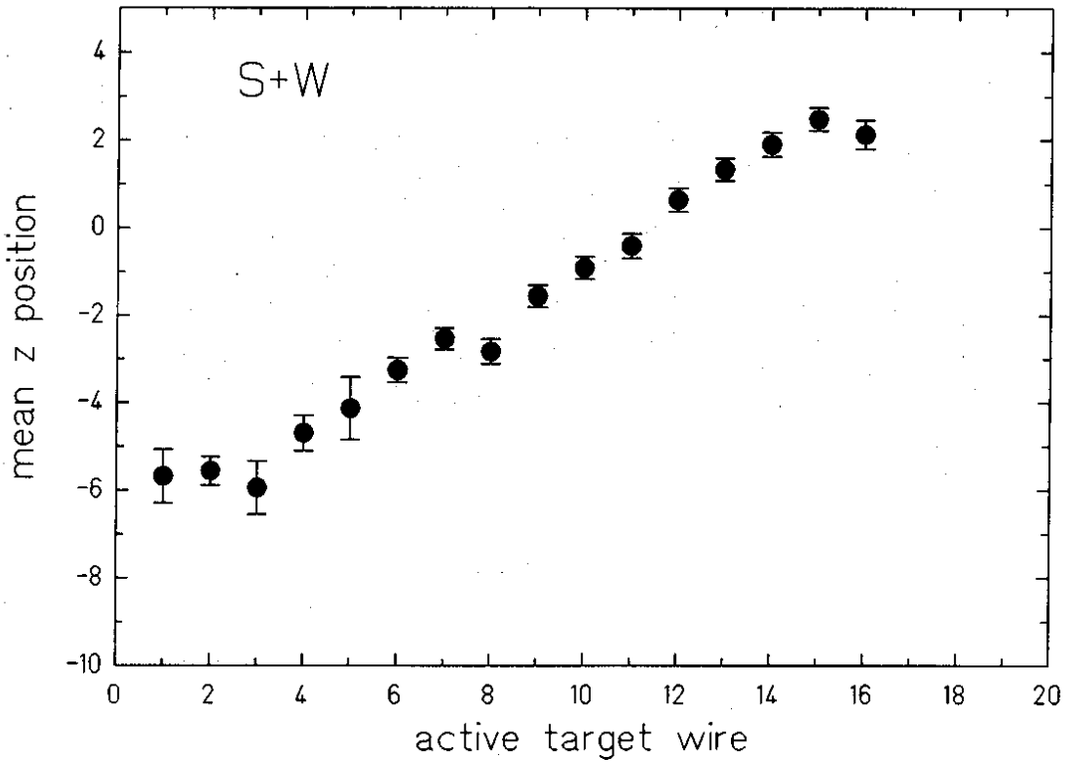
S+W
mean z position
active target wire

Fig. 2

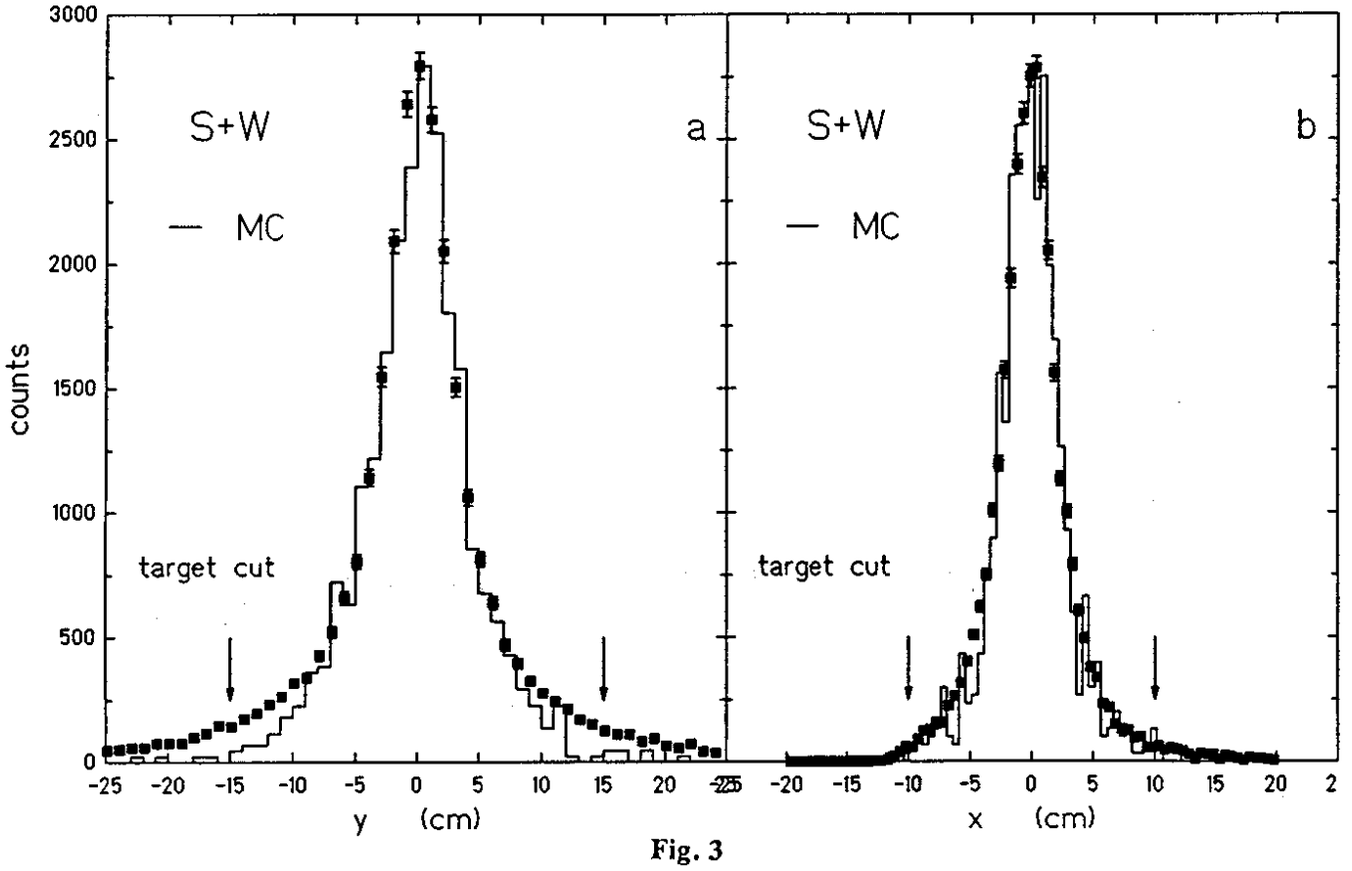
S+W
MC
a
target cut
S+W
MC
b
target cut
counts
y (cm)
x (cm)

Fig. 3

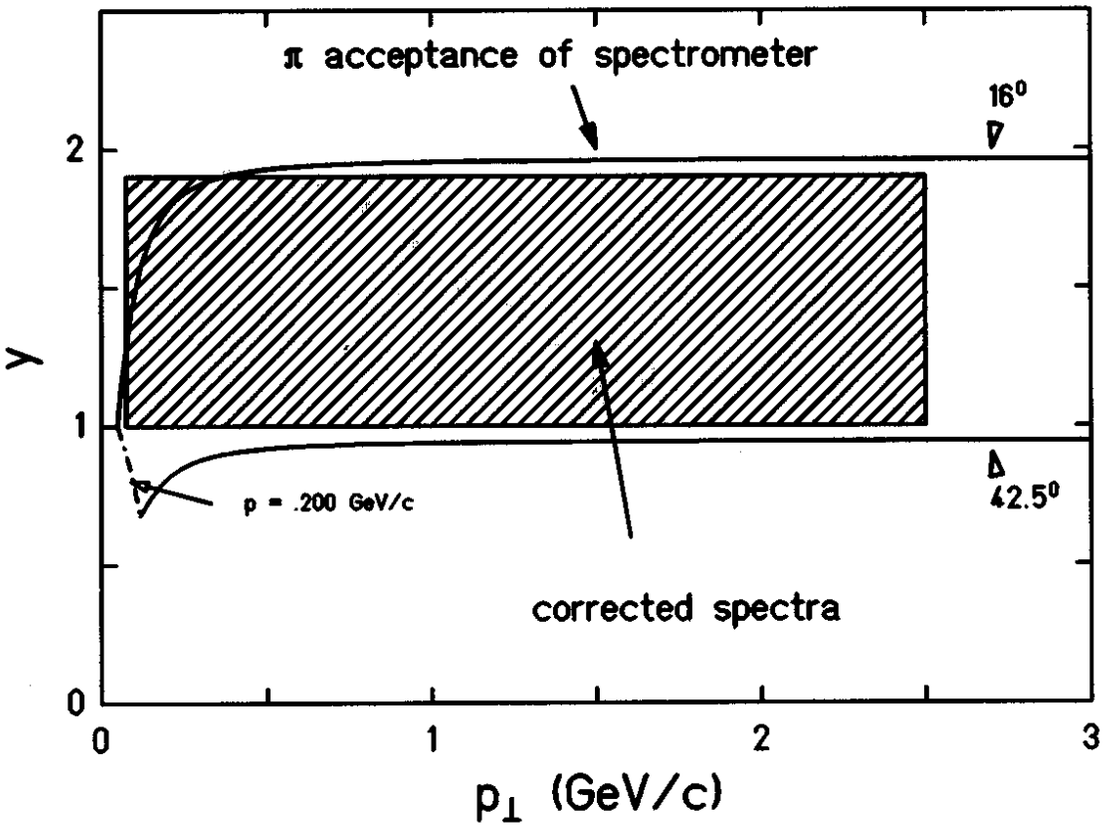
π acceptance of spectrometer
16°
42.5°
p = .200 GeV/c
corrected spectra
y
p⊥ (GeV/c)

Fig. 4

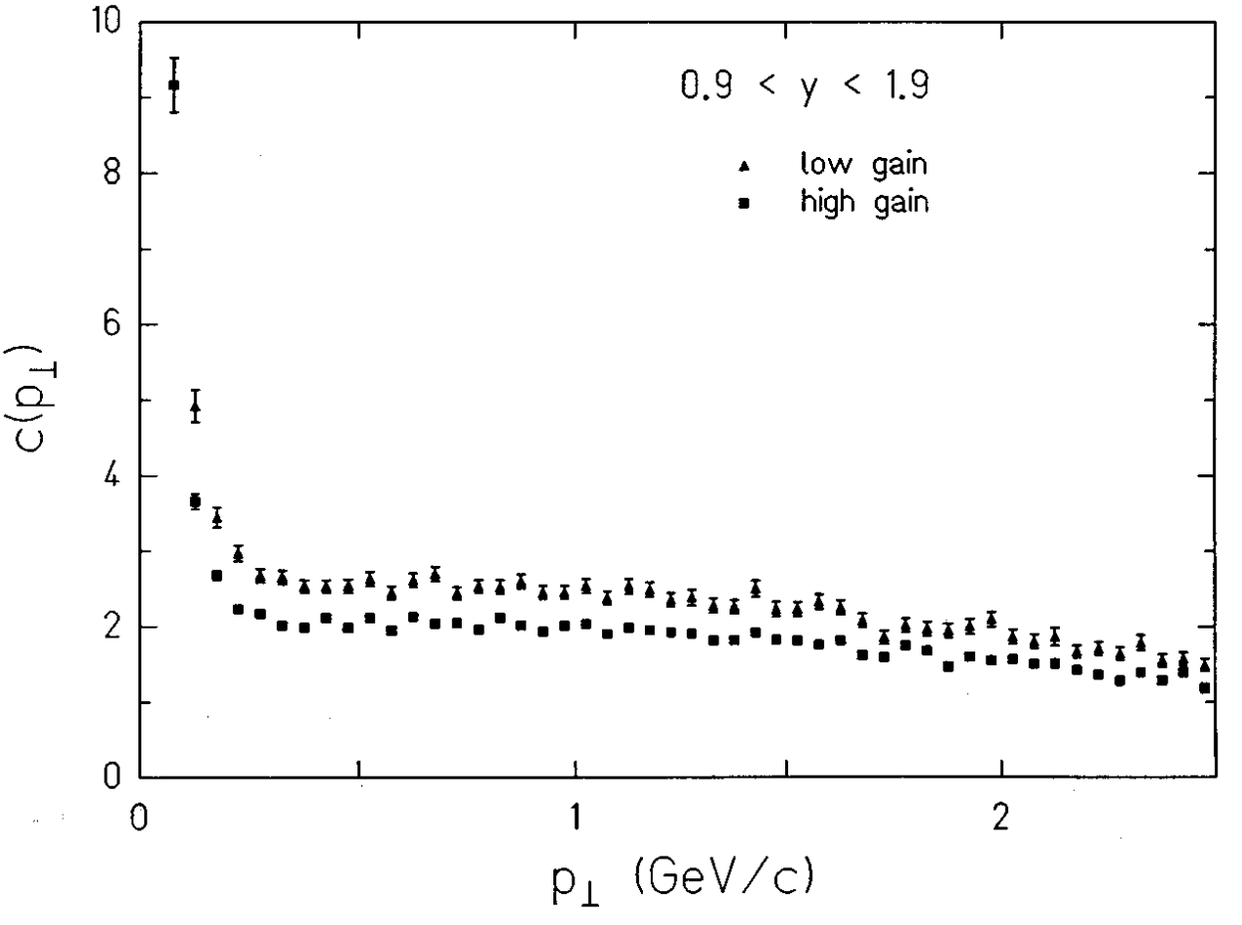
0.9 < y < 1.9
low gain
high gain
c(p⊥)
p⊥ (GeV/c)

Fig. 5

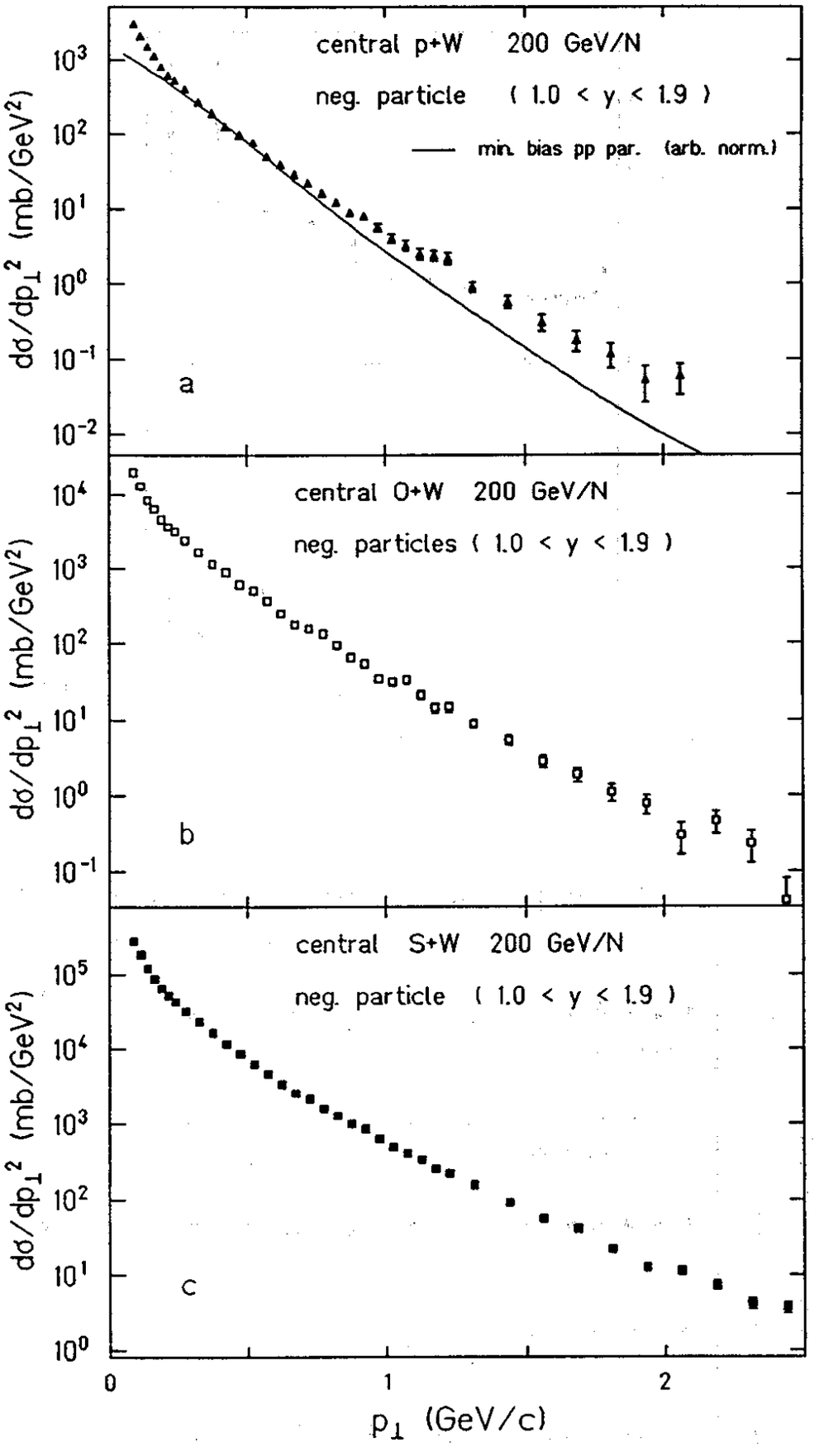
central p+W 200 GeV/N
neg. particle (1.0 < y < 1.9)
min. bias pp par. (arb. norm.)
a
central O+W 200 GeV/N
neg. particles (1.0 < y < 1.9)
b
central S+W 200 GeV/N
neg. particle (1.0 < y < 1.9)
c
dσ/dp⊥² (mb/GeV²)
p⊥ (GeV/c)

Fig. 6

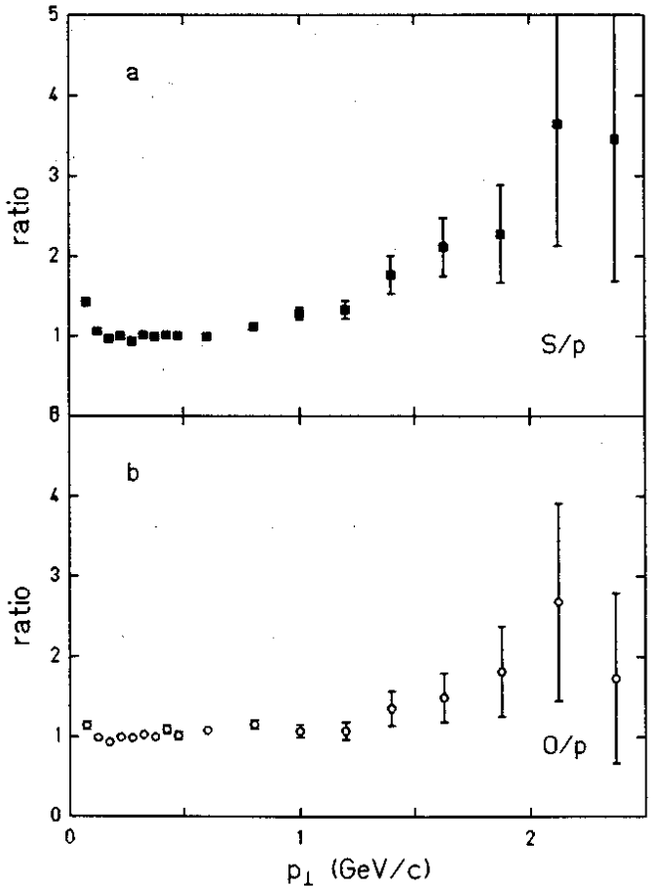
a
ratio
S/p
b
ratio
O/p
$p_\perp$ (GeV/c)

Fig. 7

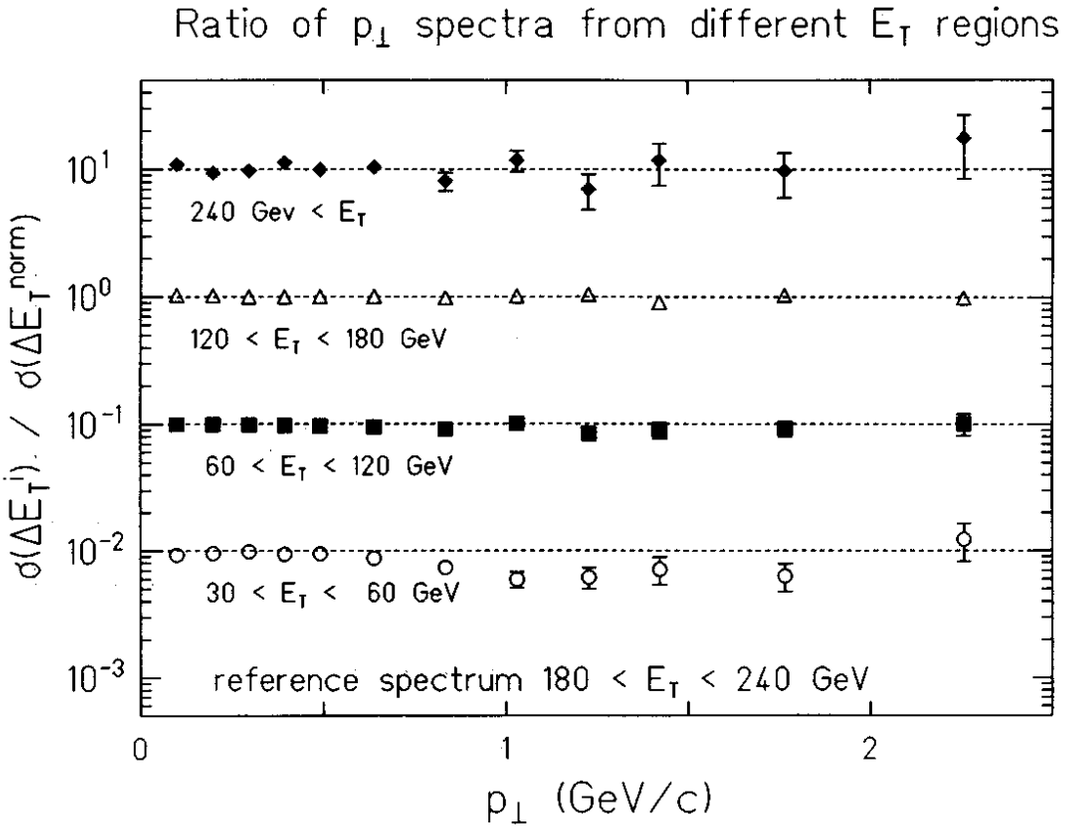
Ratio of $p_\perp$ spectra from different E_T regions
$\sigma(\Delta E_T^i) / \sigma(\Delta E_T^{norm})$
240 Gev < E_T
120 < E_T < 180 GeV
60 < E_T < 120 GeV
30 < E_T < 60 GeV
reference spectrum 180 < E_T < 240 GeV
$p_\perp$ (GeV/c)

Fig. 8

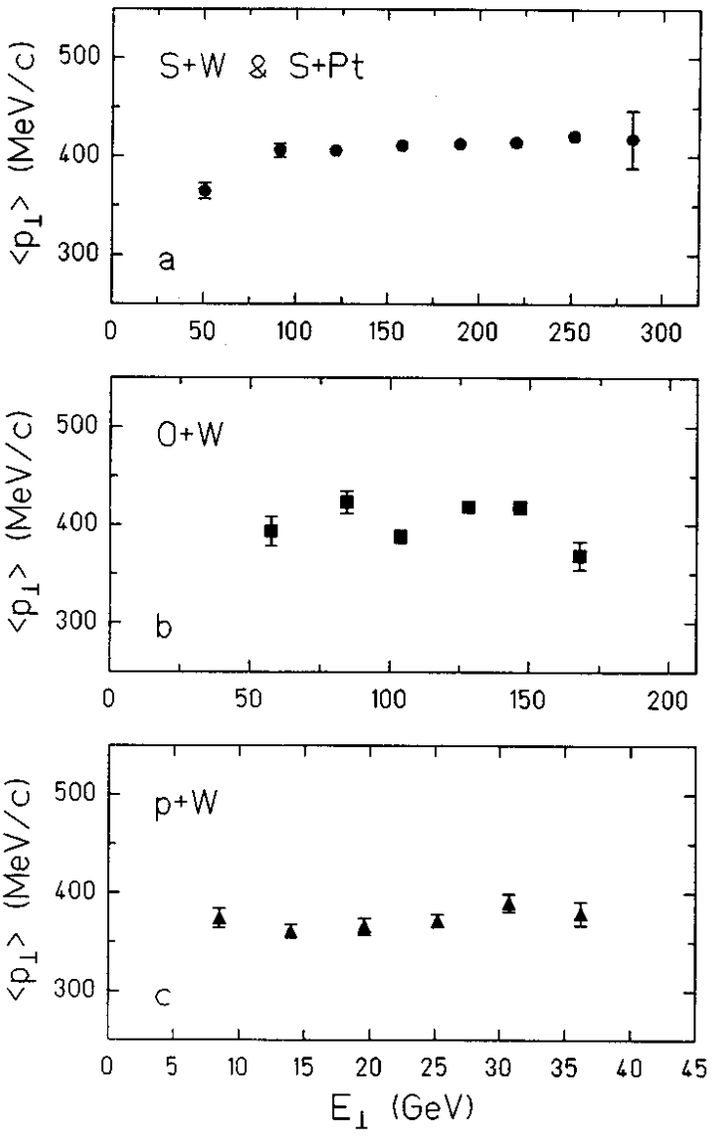

Fig. 9

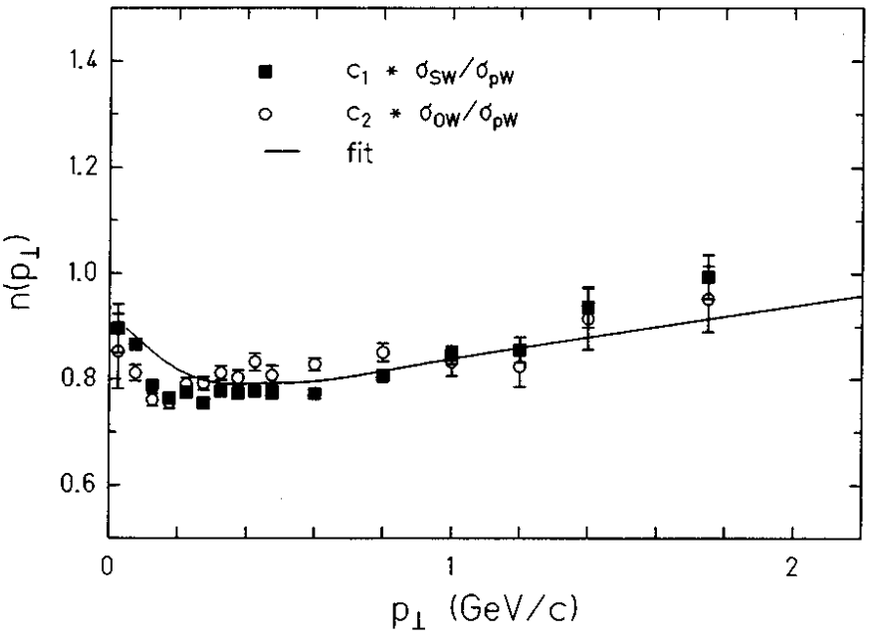

Fig. 10